ARTICLE **OPEN**

Antioxidant high-conductivity copper paste for low-cost flexible printed electronics

Shuqing Hong[1,3], Chimin Liu[1,3], Shuqiang Hao[1,3], Wenxing Fu[2], Jian Peng[1], Binghui Wu[1,2]✉ and Nanfeng Zheng[1,2]

The flexible printed electronics (e.g., wearable devices, roll-up displays, heating circuits, radio frequency identification (RFID) tags) calls for high-conductivity and low-cost materials, particularly for copper pastes. It is still a big challenge to develop reliable copper pastes for both antioxidant and high-conductivity flexible printed films and lines. In this work, an antioxidant copper paste was achieved using copper microflakes with surface passivation by formate ions and thiols, with high conductivity of 13400 S cm^{-1} (the same order of magnitude of silver pastes, 1.8–2.5 × 10^4 S cm^{-1}). The universal applications of as-prepared copper paste in flexible printed electronics (e.g., electromagnetic interference (EMI) shielding films, anti-fog films, and RFID tags) via screen printing and curing at 170 °C under ambient atmosphere were demonstrated. The as-printed electronics showed high performance in flexibility, stability, and reliability. This work shows the great potential of anti-oxidation copper pastes in low-cost flexible printed electronics for commercial usage.

npj Flexible Electronics (2022)6:17 ; https://doi.org/10.1038/s41528-022-00151-1

INTRODUCTION

Flexible electronics are increasingly gaining research interest in recent years[1–11]. A variety of flexible devices, such as wearable devices, roll-up displays, LEDs, solar cells, and RFID tags, have been developed by printing technologies[12–14]. To print flexible electronics, some ideal technologies such as screen printing have been extensively considered and adopted due to low capital cost, low pollution, and easy operation, but lack of printable, low-cost, and highly conductive materials and inks/pastes with suitable solubility, viscosity and surface tension[15,16]. Various kinds of materials such as graphene[15,17], carbon nanotubes[18], conducting polymers (CPs)[19–21], silver pastes[13,22–26], and copper pastes[27,28] have been used in printed flexible electronics. As for carbon-based materials and CPs, they have an advantage for low cost, but the conductivity of corresponding inks/pastes is relatively low. Several studies have focused on enhancing the electrical conductivity of solution-based CPs using the addition of carbon materials. For example, Lee et al.[20] worked out the carbon/polyaniline-based paste, but with a low conductivity of 792 S cm^{-1}. As for silver pastes, a lot of attention have been paid for fabricating high-quality flexible electronics because of its outstanding conductivity and oxidation resistance. However, the high price of such material limits large-scale electronics applications. In view of above-mentioned problems, metallic copper pastes can be a good alternative for conducting material because of its low cost and high intrinsic electrical conductivity. Nevertheless, copper pastes intrinsically suffer from high susceptibility to surface oxidation upon air, high temperature, and chemicals. Thus, the only way to realize practical usage of copper pastes is to possess the anti-oxidation and high-conductivity performances in a high-efficiency and low-cost way.

Many methods have been attempted to prepare high-conductivity low-cost copper pastes. The preparation process of copper pastes includes two common routes: (1) removing the surface oxide layers of copper powders and preparing the corresponding pastes with the addition of corrosion inhibitors. Commonly, acid treatments[27,29] for copper micro-scale powders are developed using acids (e.g., hydrochloric acid (HCl) and phosphoric acid (H_3PO_4)) as chemical etching and polishing agents to make a clean, oxide-free surface of copper[27]. The cleaned copper micro-scale powders were mixed in a short time with corrosion inhibitors and others to form so-called anti-oxidation copper pastes. For the nano-scale copper paste, especially Cu nanoparticle inks with corrosion inhibitors, Cu nanowires were added to improve the electrical conductivity and reliability of flash light-sintered Cu films[30]. Although flash light-mediated processes are promising for air sintering of Cu-based inks, these approaches require expensive and specific equipment. To solve these issues, Mai et al.[31] have demonstrated air-atmosphere sintering at low temperature using a novel Cu-based composite ink with sub-10 nm Cu nanoparticles. The preparation of sub-10 nm copper particles was complicated with potential high cost. However, the long-term usage of above pastes was rarely reported due to the insufficient protection strategy. (2) Synthesizing the anti-oxidation copper powders with protection layers and directly preparing the corresponding pastes with solvents and additives. For the protection methods of copper powders, protective coating layers[32–35] (e.g., silver capping layer, imidazole-based molecules, organic thiols) have been generally adopted to prevent oxidation under ambient conditions. In both routes, conductive films based above copper pastes have been developed (Supplementary Table 1)[31,36–38]. Although those reported methods have somehow improved the anti-oxidation and conductivity property of copper pastes, those copper pastes still suffered from insufficient antioxidation protection or complex preparation process or high cost, limiting their wide industrial applications.

Recently, we have principally revealed the passivation role of formate ions (and organic thiols) on copper foils via a highly

[1]Pen-Tung Sah Institute of Micro-Nano Science and Technology, State Key Laboratory for Physical Chemistry of Solid Surfaces, Collaborative Innovation Center of Chemistry for Energy Materials, National & Local Joint Engineering Research Center of Preparation Technology of Nanomaterials, College of Chemistry and Chemical Engineering, Xiamen University, Xiamen 361005, China. [2]Innovation Laboratory for Sciences and Technologies of Energy Materials of Fujian Province (IKKEM), Xiamen 361005, China. [3]These authors contributed equally: Shuqing Hong, Chimin Liu, Shuqiang Hao. ✉email: binghuiwu@xmu.edu.cn

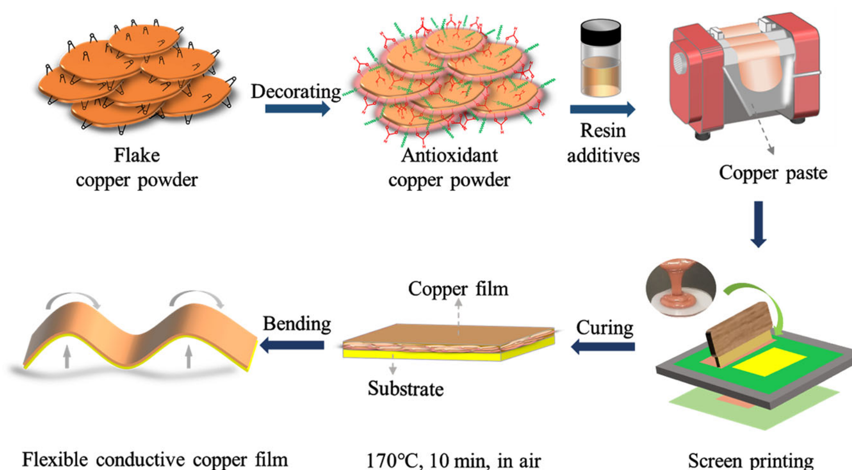

Fig. 1 General scheme for fabricating antioxidant copper paste and screen printing flexible electronics. The entire process to prepare the flexible electronics includes: decorating the flake copper powder, mixing & grinding the copper powder and solvent (containing resin additives and others), screen printing on flexible substrates, and curing the wet films in air at 170 °C for 10 min to form final flexible conductive films.

efficient, universal, and low-cost method for oxidation resistance[39]. In this paper, this surface passivation strategy was intensively adopted on copper powders, with which antioxidant copper paste of high conductivity and long-term stability was further developed and realized via a simple, scalable and economic way. The copper powder of microflakes was protected with formate ions (FA) and dodecyl mercaptan (DT) to form a protective layer, evolved according to our recent report[39]. The as-prepared antioxidant copper paste could be screen printed and cured in air at 170 °C for 10 min, with a conductivity up to 13400 S cm^{-1}. EMI shielding films, anti-fog films, and RFID tags were fabricated as examples of applications. All these applications demonstrated the great potential of anti-oxidation copper paste in low-cost flexible printed electronics for commercial usage.

RESULTS AND DISCUSSION

Anti-oxidative protection of copper powder

Copper powder in the shape of microflakes was first treated and passivated by a mixed molecular layer of FA and DT, and then used as conductive filler in the preparation of antioxidation copper paste and high-conductivity copper films by screen printing for flexible electronics study (Fig. 1). The surface passivation process of commercial copper microflakes (average 80 nm in thickness and 3 μm in lateral size) was detailly described in the "Experimental Section/Methods"[39]. The untreated powder was denoted as Cu-None and as-treated copper powder as Cu-FA/DT. As shown in Fig. 2a, b and Supplementary Fig. 1a, b, the color change was obvious from red–brown to pink, but the morphology and size of copper microflakes was almost unchanged after surface treatment. Also, the electrical conductivity of Cu-FA/DT powder was almost unchanged after the 0.1 M NaOH corrosion test compare to Cu-None powder (Supplementary Fig. 1c). This indicated that the surface passivation happened on copper microflakes. As discussed in our previous paper[39], the thin oxide layer on copper surface was converted into the structure of $[Cu(\mu\text{-}HCOO)(OH)_2]_2$. The integration of FA and adscititious thiol would endow copper powders with oxidation resistance, ready for the direct preparation of high-conductivity pastes for the latter study.

The successful surface decoration and protection of FA and DT on copper powders were demonstrated by the characterization of surface species via Raman/FTIR spectra and alkali resistance test in strong base: (1) As shown in Raman spectra (Fig. 2e), there was no obvious characteristic peak on the surface of copper powder before anti-oxidative decoration, while the characteristic peak of (–OCO–) appeared at 1566 cm^{-1} position and (–CH–) characteristic peak appeared at 2934 cm^{-1} of copper powder after anti-oxidative decoration[29,40]. The organic species with (–OCO–) and (–CH–) were assigned to $HCOO^{-}$[41]. And the thiol molecules were identified by IR spectra (Supplementary Fig. 1d). These confirmed the successful decoration of FA and DT on copper microflakes. (2) The alkali resistance test was carried out in 0.1 mol L^{-1} NaOH aqueous solution (pH = 13) at room temperature for 24 h. The surface of Cu-None powder after the test was covered with needle-like 'flowers' (Fig. 2c), which were Cu_2O and CuO species verified by the Raman peaks at (147, 213) cm^{-1} and (417, 628) cm^{-1} (Fig. 2f), and the XRD patterns showed the presence of 36.4° and 38.5° peaks in XRD patterns (Fig. 2g, h), respectively. While the surface of Cu-FA/DT powder kept unchanged after alkali resistance test (Fig. 2d), the anti-corrosion results of Cu-FA/DT powder indicated the strong binding of FA and DT on copper microflakes. In summary, the presence of FA/DT and their strong binding on copper microflakes endowed the as-prepared Cu-FA/DT powder with attractive anti-corrosion and anti-oxidation capacity, which were ready for the fabrication of anti-oxidation high-conductivity copper paste for further studies.

Preparation and properties of copper paste

The anti-oxidation copper powders with FA/DT protection layers were directly used for preparing the corresponding pastes with solvents and additives. The optimized copper paste was composed of above Cu-FA/DT powder, phenol resin, triethanolamine (TEOA), and 2-Amino-2-methyl-1-propanol (AMP) as both solvents and curing agents, dimethyl carbonate as an additive agent to enhance flexibility[42,43]. In the field of conductive pastes, it is common and convenient to use the mass ratio to quantify each component; in our case, the optimum mass ratio was 50:22:15:11:2, which was shown in the Methods section. More specifically, phenol resin afforded the conductive copper paste with adhesiveness and curability, as well as outstanding thermosetting shrinkage to ensure intimate contact among copper microflakes[44]. Triethanolamine immobilized the copper powder, and suppressed the active effect of the carboxyl groups of the formate under room temperature. Both TEOA and AMP was used to cure the phenol resin at elevated temperature. Accordingly, the Cu-FA/DT powder was well dispersed in the matrix of organic phase, resulting in homogeneous antioxidant copper paste (Fig. 3a) with high screen-printing capability. The copper paste was

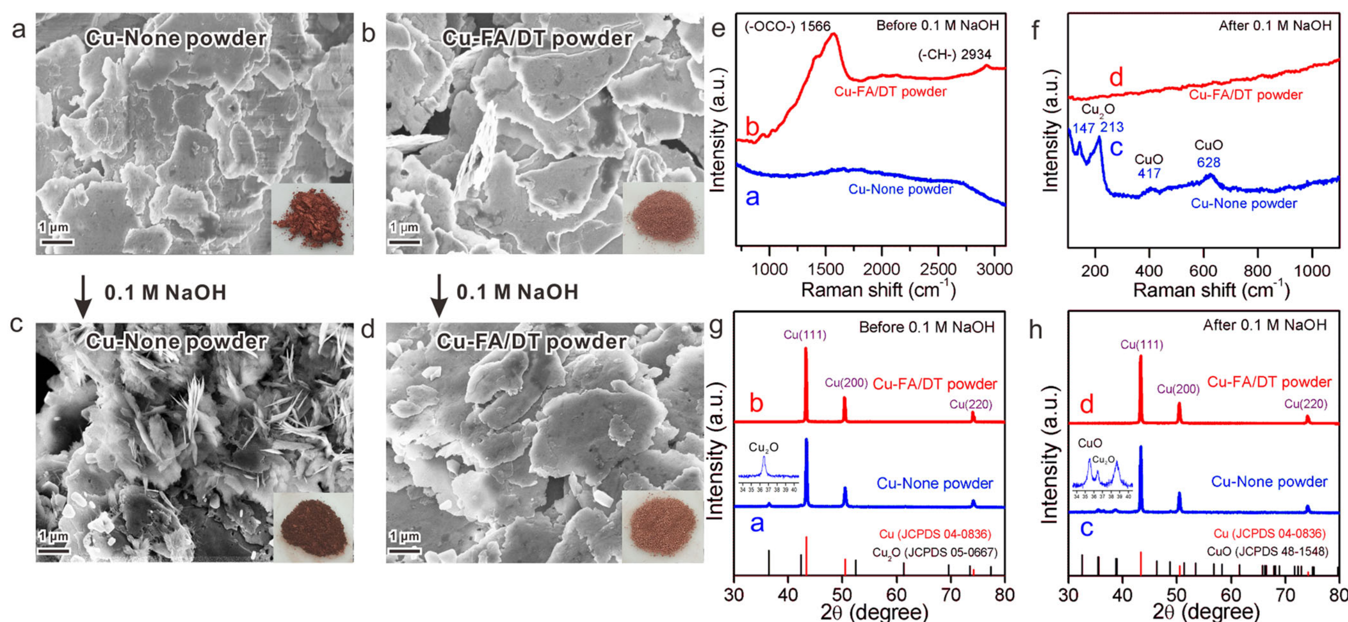

Fig. 2 Effects of FA/DT surface passivation on commercial copper microflakes. Copper powder before and after alkali resistance test in 0.1 M NaOH at room temperature for 24 h. SEM images of **a**, **c** Cu-None powder and **b**, **d** Cu-FA/DT. Raman spectra of Cu-None powder, Cu-FA/DT powder before (**e**) and after (**f**) the alkali resistance test. XRD patterns of Cu-None powder, Cu-FA/DT powder before (**g**) and after (**h**) the alkali resistance test.

curable in an ambient atmosphere and inert gas (e.g., N_2) was not needed. The best temperature was no lower than 170 °C to cure our copper paste to reach high conductivity (Supplementary Fig. 2 and Supplementary Table 2). Voids or pin holes among copper powder were eliminated by the shrinkage of phenolic-formaldehyde resin during the curing process at 170 °C (Supplementary Fig. 2b, c and Fig. 3a) and the total solid content (copper powder, 50 wt.% (Supplementary Fig. 3b), and cured phenol resin) of the paste was up to 72.58 wt.% after fully cured (Supplementary Fig. 3c). The adhesion ability of printed films could reach 5B level (Supplementary Fig. 3d), measured according to the international standard of ISO 2409-92. Consequently, the Cu-FA/DT paste with optimized content of solvent and resin possessed suitable viscosity (12500 cP at 20 °C) and rheological property, endowing the cured films with high mechanical property, as well as strong adhesion to the substrates (e.g., polyimide-PI, polyethylene terephthalate-PET, glass).

The Cu-FA/DT paste with shrinkable polymer resin also ensured the cured films with continuous conducting paths for high conductivity and oxidation resistance. To verify the anti-oxidation ability of conductive Cu-FA/DT films prepared by surface-decorated copper powder in an ambient atmosphere, a comparative test was examined with conductive films prepared by pristine copper powder (Cu-None film) as shown in Fig. 3b. The sheet resistance of Cu-None film increased by 6464 times from 4 Ω sq^{-1} @25 μm to 25856 Ω sq^{-1} @25 μm after 2160-h storage at room temperature. However, the sheet resistance of Cu-FA/DT film was basically maintained at around 30 mΩ sq^{-1} @25 μm. Additionally, the Cu-FA/DT film showed its stability at 60 °C (Fig. 3c): the initial sheet resistance of Cu-FA/DT film was 28.91 mΩ sq^{-1} @25 μm, and it was 29.80 mΩ sq^{-1} @25 μm after 480 h. These results confirmed the attractive conductivity and anti-oxidant capacity of the Cu-FA/DT films made from Cu-FA/DT paste.

The mechanical, conductive, and antioxidant properties of the cured Cu-FA/DT films were further comprehensively studied. Here, lines with various widths were firstly screen printed and cured together on PI substrate, using Cu-FA/DT paste (Fig. 3d). The printability and uniformity of copper paste on substrate are the key indexes to evaluate the quality of screen printing. Under certain condition by screen printing, the thickness of printed lines was about 25 μm when the line width was greater than 1.0 mm (Fig. 3e). When the width of printed line was less than 1.0 mm, the printing thickness decreased with the decrease of line width. The measured electrical resistance of conductive lines of different lengths and various line widths were showed in Fig. 3f. Obviously, it exhibited a high linear correlation between line length and resistance, and the resistance decreased as the printed line width increased. These results are well fitted to the definition of electrical resistance: $R = \rho L\ S^{-1}$, where ρ, L, S are the resistivity, length, cross-sectional area, respectively. And the electrical conductivity of printed lines was higher than 10^4 S cm^{-1} (an average of 13400 S cm^{-1}), much better than previously published papers (Supplementary Table 1)[27,32,33]. Note that it is specific for using formate and dodecyl mercaptan to protect copper powder to realize the highest conductivity of final copper paste (Supplementary Table 3).

The flexible property was characterized via bending test on the screen-printed conductive lines with different widths (Fig. 3g–i). The relative electrical resistance ($\Delta R/R_0$) of printed lines was plotted vs bending cycles (Fig. 3h), which was almost unchanged with the line width higher than 0.5 mm. While the relative electrical resistance slightly increased with the decrease of the line width below 0.5 mm, and the maximum $\Delta R/R_0$ of the finest line (0.2 mm in width) we tested was not beyond 5% after 500 times of bending. When plotting the $\Delta R/R_0$ value after 500 bending cycles as a function of line width (Fig. 3i), it was found that our Cu-FA/DT paste was equivalent to commercial flake-like silver paste. For comparison, spherical copper paste was prepared using similar FA anti-oxidative protection and with the same content of organic phase. The $\Delta R/R_0$ of lines printed by flake copper paste and spherical copper paste after 500 times bending cycles (Supplementary Fig. 4) confirmed the superior in choosing microflake-like copper for study. Therefore, by integration of flake-like Cu-FA/DT and phenol resin, the Cu-FA/DT films and lines made from Cu-FA/DT paste had outstanding mechanical, conductive, and antioxidant properties, ready for the development of low-cost flexible printed electronics.

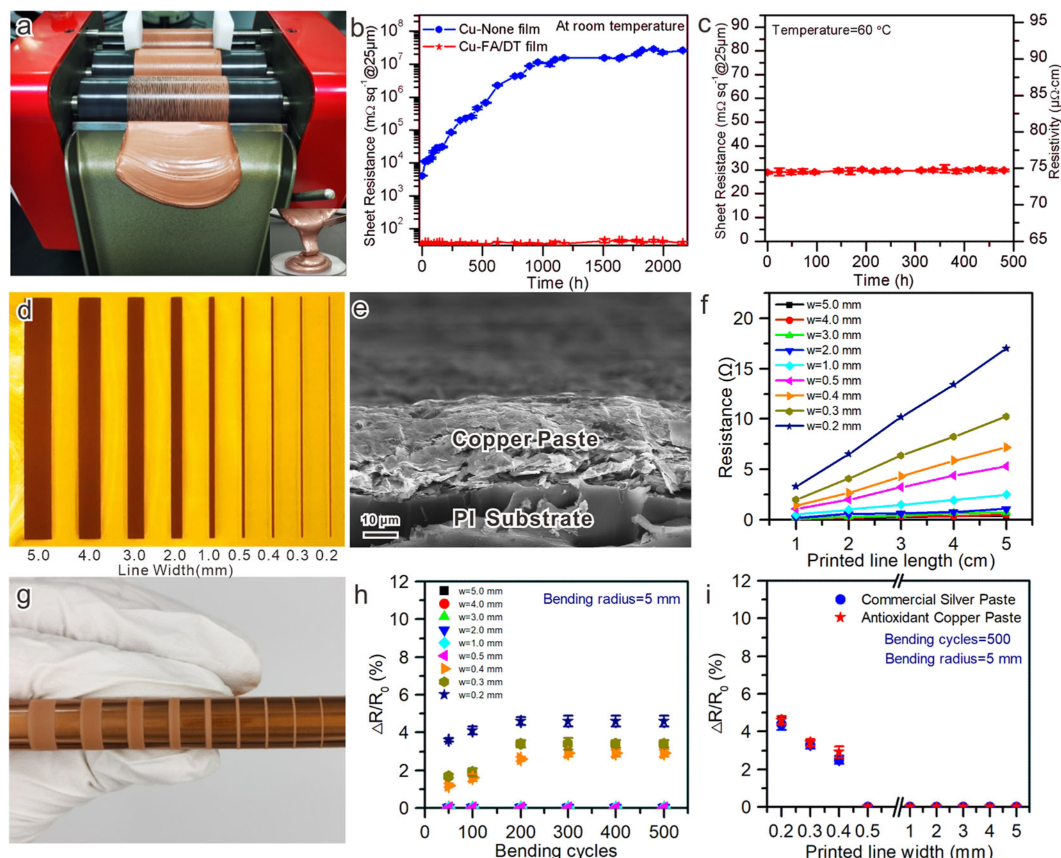

Fig. 3 Electrical and mechanical properties of the antioxidant copper paste. a Optical images of the copper paste prepared by a three-roll grinder. **b** Long-time stability of copper films at room temperature. **c** Long-time stability of the Cu-FA/DT film at 60 °C. **d** Optical image of lines screen-printed on PI substrate with different widths. **e** Cross-sectional SEM image of the printed line with 1.0 mm width. **f** Electrical resistance of the printed conductive lines as a function of line widths. **g** Bending test on a cylindrical rod with a radius of 5 mm. **h** Relative electrical resistance of the printed conductive lines on PI during 500 bending cycles at a bending radius of 5 mm. **i** Relative electrical resistance of various conductive lines on PI printed by different conductive pastes after 500 bending cycles.

Flexible printed electronics of copper paste

As discussed in the above sections, the as-prepared antioxidant copper paste had attractive printable, electrical, and mechanical properties, and was expected to be printed for high-performance flexible electronics. In this work, all-printed EMI (electromagnetic interference) shielding films, anti-fog heating films, and RFID tag antennae were fabricated and characterized to prove the feasibility and universality of copper paste applied in flexible printed electronics.

EMI shielding films

Flexible films with high conductivity but minimal thickness is highly desirable to provide EMI shielding in many fields[45]. Here, EMI shielding films (Fig. 4a, b) were fabricated by screen-printing copper paste on a PI substrate. The EMI shielding effectiveness (SE) can be altered by the film thickness. As proved in Fig. 4c, the SE showed a slightly positive correlation with the film thickness, when the thickness was beyond 15 μm. The slight enhance in EMI SE was due to the multiple reflection of electromagnetic wave caused by laminate structure of copper paste. When a 35 μm-thick film made from copper paste was tested, an EMI SE value up to 68.8 dB at 3.5 GHz was recorded, enough to block 99.9999% of incident radiation with only 0.0001% transmission[45]. A 35 μm-thick film from silver paste was also tested, demonstrating similar shielding capacity and mechanism (Supplementary Fig. 5). Note that the EMI SE of films made from copper paste reached the same value of silver paste.

To obtain better EMI SE, the EMI shielding bilayer films from flake copper paste and graphene ink were also prepared (Fig. 4d). The films made from commercial graphene ink (Fig. 4e) and our copper paste (Fig. 4f) possesses a superb electrical conductivity of 30 mΩ sq^{-1} @25 μm (copper side) and 3.4 Ω sq^{-1} @25 μm (graphene side). The conductivity was calculated by the sheet resistance and film thickness. Figure 4g shows that the SE of 8 μm single graphene film was around 30.6 dB @ 3.5 GHz, and that for 35 μm single copper film was 68.8 dB @ 3.5 GHz. To our surprise, the EMI shielding bilayer film (totally 43 μm) from both graphene ink and flake copper paste could be promoted to 80.3 dB (much higher than that of 45 μm copper film), enough to block more than 99.99999% of incident radiation. This may be attributed to the synergistic effect between copper and graphene[46]. This finding was similar to the previous reports[47]. We believe that other two-dimensional materials with intrinsic EMI property can be integrated with our copper paste to reach a maximum EMI shielding. A comprehensive literature review of previously studied materials for EMI SE (Supplementary Table 4)[45,48–53] clearly indicates that the copper paste is an outstanding candidate for EMI shielding materials.

Electric heating anti-fog films

Transparent films and substrates with electric circuits in the camera or mirror are supposed to be heated to eliminate the temperature difference between films and the environment, that is to prevent fogging caused by the temperature difference between cold and hot[54,55]. Here, anti-fog flexible films were

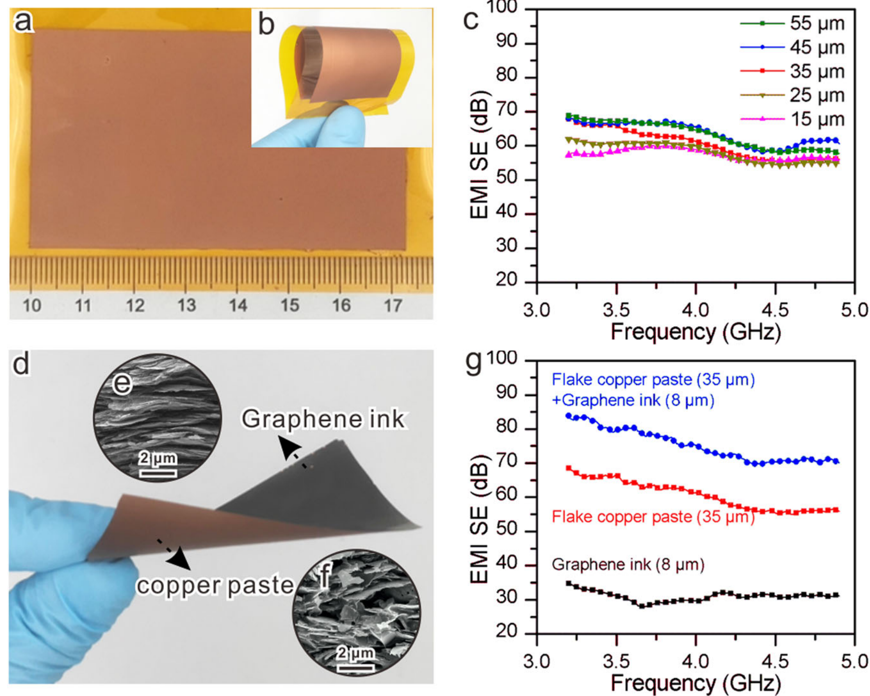

Fig. 4 Characterization of EMI shielding films. a Image of the film printed with copper paste on PI substrate. **b** Bending display of the film. **c** EMI SE of copper paste films at different thicknesses. **d** Image of the film printed with flake copper paste and graphene ink. **e** Cross-sectional SEM image of the graphene ink layer. **f** Cross-sectional SEM image of the copper paste layer. **g** EMI SE of films printed with different materials.

fabricated by screen-printing copper paste on a PET substrate with a designed circuit (Fig. 5a).

Detailed studies on the performance of our anti-fog films were carried out. Firstly, the cold and hot shock tests on the encapsulated films at −20 to +60 °C under the heating voltage of 4 V were performed to verify the stable operation of the anti-fog films with copper-based heating circuit. After 8 cycles of shock tests, the resistance of copper-based heating circuits was basically stable, and the heating capacity could be maintained in ambient conditions since the center temperature of the films at 4 V unchanged (Fig. 5b). The center temperature was dependent on the applied higher voltage, confirmed by Fig. 5c. Also, the power and center temperature were maintained after continuous test of 6 days, indicating the stability under different voltages. The average temperatures of films corresponding to the input voltages of 4, 8, and 12 V were 34.9, 39.2, and 41.6 °C, respectively (Fig. 5d–f). The anti-fogging effect was demonstrated according the Chinese test standard for anti-fogging plastic film (GB/T 31726-2015) (Fig. 5g–i). Upon covering the film on 80 °C hot water, the fog was immediately formed on the bottom, and then disappeared in 30 s after charging the film at 5 V. This result confirms the potential of flexible heating circuits and electronics based on our antioxidant copper paste.

RFID tags

Common passive RFID tags can be divided into high-frequency (HF, 13.56 MHz) tags and ultra-high-frequency (UHF, 915 MHz) tags according to their working frequency[10,15,17]. HF tags are suitable for short-range identification, while UHF tags for long-range identification. In this work, the design, printing, and research of RFID tags based on antioxidant copper paste were carried out and demonstrated to be suitable for different frequencies and different occasions.

The HF RFID tags were provided by including HF coil antennae printed with copper paste flexible (PI) substrate, HF RFID IC chips, copper tape for bridge connection, as shown in Fig. 6a. The tag antennae with different number of coils were designed and fabricated. For the convenience of comparison, the length and width of outer-ring antennae were all chosen as 80 and 50 cm, respectively, and the line width and line spacing were all chosen as 1 and 0.5 mm, respectively (Supplementary Fig. 6a). The number of the coils was chosen from 4 to 9. The HFSS software was used to calculate the inductance of antennae. The comparison between the calculated and measured inductance of the fabricated tag antennae was presented in Fig. 6b, indicating that the measured inductance data of antennae with different number of coils was consistent with the calculated one. Preferably, the inductance of 8-coil antennae was most suitable for the resonance condition, and the reading range of 8-coil antennae was up to 4.5 cm (Fig. 6b). In addition, the fabricated tags could be bent or twisted during our test. After bending an 8-coil HF tag at a bending radius of 5 mm for 500 cycles, the $\Delta R/R_0$ value was almost zero, and the reading range was unchanged (Supplementary Fig. 6b). To further verify the stability of the fabricated antennae, a comparative test was examined on the long-term resistance and reading range of tags fabricated by antioxidant copper paste and commercial silver paste with 8 coils (Fig. 6c). The resistance of copper paste antennae and the reading range of corresponding tags were unchanged after storing for 70 days. In addition, the $\Delta R/R_0$ of tag antennae printed by antioxidant copper paste was basically equal to that by commercial silver paste during the cycling test from −20 to +60 °C for 6 h (Supplementary Fig. 6c). The above results demonstrated that the antioxidant copper paste had great potential to replace silver paste in the application of HF RFID tags.

For the UHF RFID tags, each consists of two main components: a UHF antenna and an UHF RFID chip attached to the antenna. The antenna design was first performed on the HFSS software to simulate the antenna model, and an optimized model was finally found through folding the arms of a dipole antenna along a meandered path (Supplementary Fig. 7a), considering the

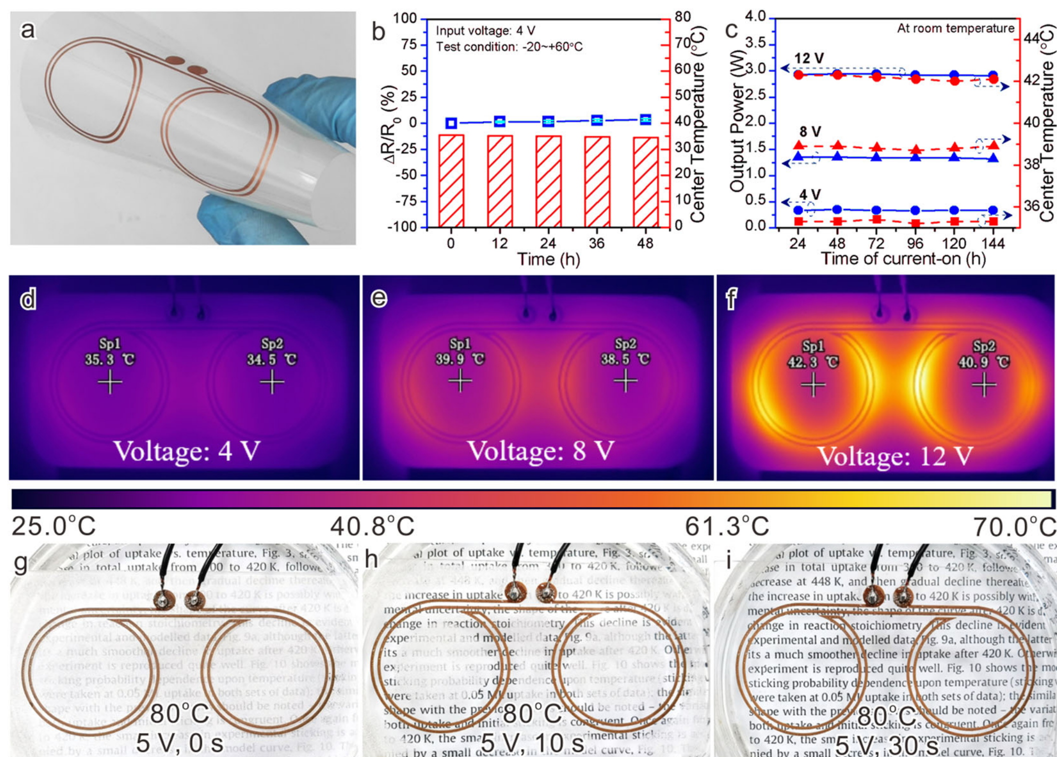

Fig. 5 Characterization of anti-fog films. **a** Flexible pattern of screen-printed copper paste conductive circuits on PET substrates. **b** Cold and hot shock tests under 4 V input voltage. **c** Output power and steady-state center temperature of the electrothermal device as a function of power-on time. IR images of the electrothermal device under **d** 4 V, **e** 8 V, and **f** 12 V input voltage. **g**–**i** Optical images of copper electric heating film, putting on 80 °C hot water with a distance of 5 cm.

impedance matching and size reduction. The printed antenna with a chip was shown in Fig. 6d. The maximum gain of the dipole antenna was −2 dB, as shown in Fig. 6e, and the two-dimensional radiation patterns of the antenna were symmetrical (Supplementary Fig. 7b, c), indicating that the virtual antenna had good omni-directivity[20]. The reflection coefficient (S_{11}) indicated how well a given tag antenna structure was matched to the attached RFID chip. And the small value of S_{11} indicated the high efficiency of the antennae. The S_{11} of a fabricated dipole antenna was −38 dB (Fig. 6f). The calculated and measured S_{11} results were in good agreement with the minimum point at a frequency of around 915 MHz. It was noted that the difference observed between the calculated and measured S_{11} values was mainly caused by the deviations between the measured and defined impedance data of the employed UHF chips. Moreover, the reading ranges of dipole tag antennae with copper paste printed on non-metal substrates (e.g., PI, paper, and textile) were about 12.8, 11.3, and 7.7 m (Supplementary Table 5), respectively, regulating with the EIRP (Equivalent Isotropic Radiated Power of reader) of 4 W. These data confirmed the realization of UHF RFID tags based on the antioxidant copper paste and their feasibility on different substrates.

The UHF tags with dipole antennae had a long recognition distance on non-metal substrates, and were further designed and improved to work on the surface of metal objects. Therefore, on-metal UHF RFID tags based on microstrip patch antennae printed with copper paste were further explored (Fig. 6g). After modeling and optimization, each on-metal RFID tag consisted of three main components: a folded-patch antenna, an UHF RFID chip attached to the antenna, and a $30 \times 30 \times 3.0\ mm^3$ soft PET foam with a dielectric constant of $\varepsilon_r = 1.03$ and a loss tangent of $\tan\delta = 0.0001$ (Supplementary Fig. 8a, b). Each antenna is composed of an E-shaped patch and a square ground plane, which could all be printed on the same layer of the unfolded PI substrate. The square ground plane was adhesive to the reverse side of the PI film, and the naked inlay was folded around the soft foam. And the maximum gain of the antennae with the optimized parameters was −8.7 dB (Supplementary Fig. 8c). Good agreement was found for the calculated result and measured result of S_{11} (Supplementary Fig. 8d), indicating that the proposed tag antenna was well conjugate-matched with the chip impedance at the resonant frequency of 915 MHz. Additionally, the S_{11} values of different conductive material-based antennae collected from previous reports[13,15,17–20,22–26] were plotted with the antenna conductivity in Fig. 6h. The as-fabricated on-metal antennae by copper paste exhibited a S_{11} value (−38 dB) lower than that of other materials with the same level conductivity (Supplementary Table 6), similar to the antennae fabricated by silver paste[25]. Moreover, the reading ranges of the microstrip patch RFID tags could reach 4.8 m when placing on an aluminum metal of 5 mm in thickness. Comprehensive comparison was listed in Supplementary Table 7 with reported on-metal tag antennae that can be found in the literature, showing the superior performance with small size. Therefore, the newly designed on-metal tags using copper paste here were simple, low-cost, flexible, and able to achieve a long reading range.

The HF tags, UHF tags, and on-metal UHF tags with reading range of 4.5 cm, 12.8 m, and 4.8 m (Table 1), respectively, were successfully realized in this work. This confirmed that the antioxidant copper paste showed a huge application prospect in various RFID-based fields.

In conclusion, we have demonstrated an effective method to fabricate antioxidant high-conductivity copper paste for printing low-cost flexible electronics under ambient conditions. The modification of formate anions and organic thiols endowed the flake-like copper powder with attractive anti-oxidation property, and also the as-prepared copper paste with high electrical conductivity ($13400\ S\ cm^{-1}$ of cured films and lines). The

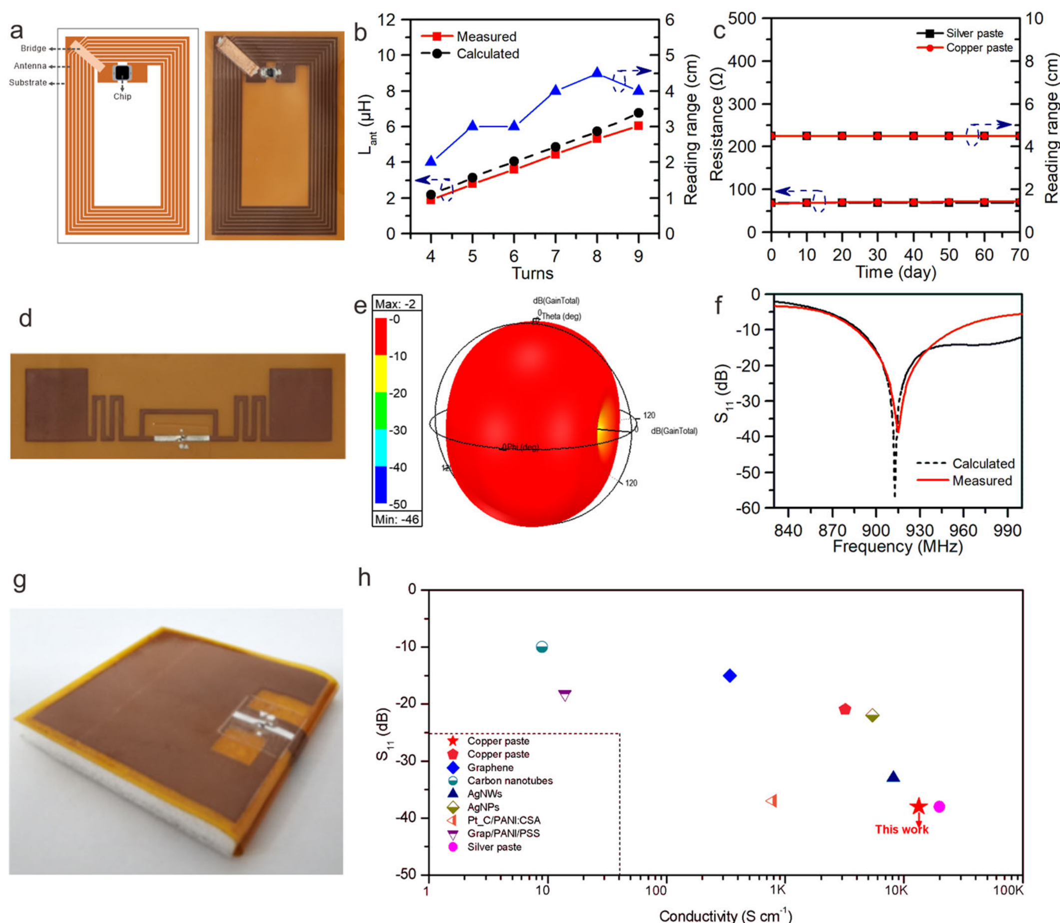

Fig. 6 Characterization of RFID tags. **a** Structure diagram (left) and physical picture (right) of HF RFID tag. **b** Calculated and measured inductance and reading range of HF RFID tag antennae affected by number of coils. **c** Comparative test on the long-term resistance and reading range of antennae with 8 coils fabricated by antioxidant copper paste and commercial silver paste. **d** Physical picture of the UHF dipole RFID tag. **e** Three-dimensional radiation pattern of the UHF dipole RFID tag antenna model calculated by HFSS. **f** Calculated and measured S_{11} results of the fabricated UHF dipole tag antennae. **g** Physical picture of the UHF microstrip patch RFID tag. **h** Comparison of S_{11} values and conductivity of antennae for different studied material with antioxidant copper paste.

antioxidant copper paste can be printed on different substrates with attractive electrical properties and mechanical properties. This allowed the achievement of outstanding performances in stability, flexibility, and economy for printed electronics (i. e. EMI films, heating circuits, and RFID antennae). Note that additional coatings[56,57] may be needed to reinforce the electronics before they can really be deployed in practice. Our work proposes an approach to utilize and optimize antioxidant copper paste for low-cost, eco-friendly, and efficient applications. Since the copper paste has a much lower cost (<20%) compared to silver paste, we believe that the real era using antioxidant copper paste instead of expensive silver one is coming.

METHODS

Materials

Copper powder (~10 μm, flake-like, ≥99.99%) was purchased from Xindun Alloy Welding Material Spraying Co., Ltd., China; ethylene glycol ($(CH_2OH)_2$, AR), sodium formate dihydrate ($HCOONa{\cdot}2H_2O$, AR), Copper(II) formate tetrahydrate ($Cu(HCOO)_2{\cdot}4H_2O$), ethyl alcohol (C_2H_5OH, AR), sodium hydroxide (NaOH, AR) and sodium chloride (NaCl, AR) from Sinopharm Chemical Reagent Co., Ltd., China; oleylamine ($C_{18}H_{37}N$, 80–90%), and dimethyl carbonate (DMC) from Shanghai Aladdin Biochemical Technology Co., Ltd., China; N-dodecyl mercaptan ($C_{12}H_{26}S$, 98%) from Shanghai McLean Biochemical Technology Co., Ltd., China; phenolic resin (4200 cP at 20 °C, measured by a Brookfield (B-type) viscometer) from Dongguan Zhicheng Plastic Co., Ltd., China; triethanolamine (TEOA, AR) from Xilong Science Co., Ltd., China; 2-Amino-2-methyl-1-propanol (AMP, AR) from Shanghai Yuanye Biological Technology Co., Ltd., China. Here, $HCOONa{\cdot}2H_2O$ and $C_{12}H_{26}S$ were used for the modification of copper powder. Phenolic resin and curing agents (TEOA, AMP, etc.) were used for the preparation of copper paste. Commercial silver paste (SP-1015) was supplied by Guangdong Nanhai ETEB Technology Co., Ltd., China, which was used for comparison with copper paste. Commercial graphene ink (No. XH-H-01) was supplied by Xiamen Xihe Technology Co., Ltd., China. And the polyethylene foam was supplied by Laird Technology Co., Ltd.

Decoration of copper powder

In a typical process, $(CH_2OH)_2$ (10 mL), $HCOONa{\cdot}2H_2O$ (1 mL, 0.2 g mL^{-1}), $C_{18}H_{37}N$ (1 mL), $Cu(HCOO)_2{\cdot}4H_2O$ (10 μL, 20 mg L^{-1}) and flake copper powder (1 g) were successively added into a 30 mL hydrothermal reactor, according to our previous report (*Nature* 2020, *586*, 390). Then, the mixed solution was stirred in the closed hydrothermal reactor at 120 °C for 3 h (note that the thermal treatment temperature should be beyond 100 °C and pH value should be within 7–12 to ensure the repeatability of anti-oxidative decoration). Subsequently, the upper liquid was removed, and the copper powder at the lower layer was immersed in $C_{12}H_{26}S$ (10 mL, 1 mmol L^{-1}) for 5 min. Afterward, the copper powder was filtered and washed with C_2H_5OH for three times, and then dried in a vacuum drying oven at 60 °C for 8 h to obtain an antioxidant copper powder.

Preparation of copper paste

To obtain the antioxidant copper paste, antioxidant copper powder, phenol resin, TEOA, AMP, and DMC were mixed at mass ratio of

RFID tag type	Frequency [MHz]	Reading range	Application
HF tag	13.56	4.5 ± 0.1 cm	Short distance recognition
UHF tag	915	12.8 ± 0.2 m	Long distance recognition
On-metal UHF tag	915	4.8 ± 0.2 m	Recognition of metal objects

Table 1. Comparison of developed RFID tags fabricated with the antioxidant copper paste.

50:22:15:11:2, and then uniformly dispersed by a homogenizer. In addition, to minimize the gap between the flake-shape copper powders inside the copper paste, a three-roller grinder was vigorously used for three times (note that almost no chemical change or any oxidation occurred in this process, since the color of copper paste was not changed, and the temperature was not obviously elevated). The copper paste could be stored in a storage device for several months.

Fabrication of EMI shielding films

The EMI shielding films printed with flake copper paste were cured in air at 170 °C for 10 min. And each copper-graphene-composited EMI shielding film was composed of a graphene ink film (8 μm) and a copper paste film (35 μm). Firstly, the graphene ink was printed on the PI substrate, after curing in air at 150 °C for 30 min, the flake copper paste was printed on the cured graphene film. Finally, the copper-graphene-composited film was torn off from the PI substrate for usage.

Fabrication of anti-fog films

The anti-fog film pattern was designed in an ANSYS workbench software, and the heating circuit pattern with a thickness of 15 μm was transferred to PET (155 μm in thickness) substrate by screen printing using fabric screens with the specification of 300 mesh. After that, the samples were cured in air at 170 °C for 10 min.

Fabrication of RFID tags

The antenna models were simulated and optimized in an ANSYS HFSS software. Then, the antennae were fabricated by screen printing using fabric screens with the specification of 300 mesh. Substrates such as PI (57 μm in thickness), paper (30 μm), or textile (160 μm) were used. After the screen printing, the samples were cured in air at 170 °C for 10 min. To further demonstrate the prospective application of the antioxidant copper paste in RFID devices, fully RFID tags were fabricated. The Fudan S50 IC chips were attached to bridge the gap of the HF antennae using tiny silver/copper paste and a copper tape, and the Alien H3 IC chips were attached to bridge the narrow gap of the UHF antennae and on-metal antennae by conductive adhesive.

Characterization and measurement

Raman spectra of copper particles were measured through a Raman spectrometer (IDSpec ARCTIC). XRD patterns were acquired on a Rigaku Ultima X-ray diffractometer. Sheet resistance of various thin films was studied through four-point probe measurements (ST2558B, Suzhou Jingge Electronic Co., LTD), and the average value was present upon test at least five times. The morphology of copper powder and copper films was studied using a field-emission scanning electron microscope (ZEISS SIGMA SUPRA 55). The differential scanning calorimetry (DSC) curves were measured through a differential scanning calorimeter (DSC214). Fourier transform infrared (FTIR) spectra were recorded from 4000 to 650 cm^{-1} on a Nicolet iS50 FTIR spectrometer (Thermo Scientific Corporation) in the diffuse reflection-FTIR mode. The resistance and inductance were measured with a LCR meter (Tonghui TH2829X). The reading ranges of RFID tags and UHF RFID tags were examined with HF reader (RC522) and UHF reader (KLM930), respectively (Supplementary Fig. 9). RFID tag antennae were connected to a coaxial cable by a SMA connector, and the return loss (S_{11}) of antennae was evaluated with a vector network analyzer (ZNB8) in the frequency range from 830 to 1000 MHz. The alkali resistance test was carried out by immersing 0.1 g copper powder in NaOH solution (2 mL, 0.1 mol L^{-1}) at room temperature for 24 h. After that, the copper powder was centrifuged and washed with H_2O for three times, and then dried in a vacuum drying oven at 60 °C for 8 h. The cold and hot shock test was carried out by setting the temperature cycle program in turn as −20 °C for 2.5 h, −20 to 60 °C for 50 min, 60 °C for 2.5 h and 60 to −20 °C for 50 min.

DATA AVAILABILITY

The authors declare that the main data supporting the findings of this study are available within the article and its Supplemental material file. Extra data are available from the corresponding author upon request.

Received: 13 September 2021; Accepted: 16 February 2022;
Published online: 18 March 2022

REFERENCES

1. Chen, X., Han, X. & Shen, Q. D. PVDF-based ferroelectric polymers in modern flexible electronics. *Adv. Electron. Mater.* **3**, 1600460 (2017).
2. Ahn, B. Y. et al. Omnidirectional printing of flexible, stretchable, and spanning silver microelectrodes. *Science* **323**, 1590–1593 (2009).
3. Zhang, Y. et al. Flexible electronics based on micro/nanostructured paper. *Adv. Mater.* **30**, e1801588 (2018).
4. Li, D. D., Lai, W. Y., Zhang, Y. Z. & Huang, W. Printable transparent conductive films for flexible electronics. *Adv. Mater.* **30**, 1704738 (2018).
5. Park, S. et al. Self-powered ultra-flexible electronics via nano-grating-patterned organic photovoltaics. *Nature* **561**, 516–521 (2018).
6. Ye, D. et al. Large-scale direct-writing of aligned nanofibers for flexible electronics. *Small* **14**, e1703521 (2018).
7. Huang, S. Y., Liu, Y., Zhao, Y., Ren, Z. F. & Guo, C. F. Flexible electronics: stretchable electrodes and their future. *Adv. Funct. Mater.* **29**, 1805924 (2019).
8. Gao, W., Ota, H., Kiriya, D., Takei, K. & Javey, A. Flexible electronics toward wearable sensing. *Acc. Chem. Res.* **52**, 523–533 (2019).
9. You, R. et al. Laser fabrication of graphene-based flexible electronics. *Adv. Mater.* **32**, e1901981 (2020).
10. Khan, Y. et al. A new frontier of printed electronics: Flexible hybrid electronics. *Adv. Mater.* **32**, e1905279 (2020).
11. Stanford, M. G. et al. High-resolution laser-induced graphene. Flexible electronics beyond the visible limit. *ACS Appl. Mater. Interfaces* **12**, 10902–10907 (2020).
12. Kumar, R. et al. Self-propelled screen-printable catalytic swimmers. *RSC Adv.* **5**, 78986–78993 (2015).
13. Liang, J., Tong, K. & Pei, Q. A water-based silver-nanowire screen-print ink for the fabrication of stretchable conductors and wearable thin-film transistors. *Adv. Mater.* **28**, 5986–5996 (2016).
14. Koga, H. et al. A high-sensitivity printed antenna prepared by rapid low-temperature sintering of silver ink. *RSC Adv.* **6**, 84363–84368 (2016).
15. Shin, K. Y., Hong, J. Y. & Jang, J. Micropatterning of graphene sheets by inkjet printing and its wideband dipole-antenna application. *Adv. Mater.* **23**, 2113–2118 (2011).
16. Wang, D. R. et al. Chemical formation of soft metal electrodes for flexible and wearable electronics. *Chem. Soc. Rev.* **47**, 4611–4641 (2018).
17. Huang, X. J. et al. Binder-free highly conductive graphene laminate for low cost printed radio frequency applications. *Appl. Phys. Lett.* **106**, 203105 (2015).
18. Vacirca, N. A., McDonough, J. K., Jost, K., Gogotsi, Y. & Kurzweg, T. P. Onion-like carbon and carbon nanotube film antennas. *Appl. Phys. Lett.* **103**, 073301 (2013).
19. Shin, K. Y., Cho, S. & Jang, J. Graphene/polyaniline/poly(4-styrenesulfonate) hybrid film with uniform surface resistance and its flexible dipole tag antenna application. *Small* **9**, 3792–3798 (2013).
20. Shin, K. Y., Kim, M., Lee, J. S. & Jang, J. Highly omnidirectional and frequency controllable carbon/polyaniline-based 2D and 3D monopole antenna. *Sci. Rep.* **5**, 13615 (2015).
21. Lee, J. S. et al. Platinum-decorated carbon nanoparticle/polyaniline hybrid paste for flexible wideband dipole tag-antenna application. *J. Mater. Chem. A* **3**, 7029–7035 (2015).
22. Park, M. et al. Highly stretchable electric circuits from a composite material of silver nanoparticles and elastomeric fibres. *Nat. Nanotechnol.* **7**, 803–809 (2012).

23. Komoda, N. et al. Printed silver nanowire antennas with low signal loss at high-frequency radio. *Nanoscale* **4**, 3148–3153 (2012).
24. Song, L., Myers, A. C., Adams, J. J. & Zhu, Y. Stretchable and reversibly deformable radio frequency antennas based on silver nanowires. *ACS Appl. Mater. Interfaces* **6**, 4248–4253 (2014).
25. Inui, T., Koga, H., Nogi, M., Komoda, N. & Suganuma, K. A miniaturized flexible antenna printed on a high dielectric constant nanopaper composite. *Adv. Mater.* **27**, 1112–1116 (2015).
26. Hong, H., Hu, J. & Yan, X. UV curable conductive ink for the fabrication of textile-based conductive circuits and wearable UHF RFID tags. *ACS Appl. Mater. Interfaces* **11**, 27318–27326 (2019).
27. Shin, K. Y., Lee, J. S., Hong, J. Y. & Jang, J. One-step fabrication of a highly conductive and durable copper paste and its flexible dipole tag-antenna application. *Chem. Commun.* **50**, 3093–3096 (2014).
28. Marindra, A. M. J., Pongpaibool, P., Wallada, W. & Siwamogsatham, S. An optimized ink-reducing hollowed-out arm meander dipole antenna structure for printed RFID tags. *Int. J. Microw. Wirel. T.* **9**, 469–479 (2017).
29. Tang, Y. D., Roberts, C. A., Perkins, R. T. & Wachs, I. E. Revisiting formic acid decomposition on metallic powder catalysts: Exploding the HCOOH decomposition volcano curve. *Surf. Sci.* **650**, 103–110 (2016).
30. Joo, S. J., Park, S. H., Moon, C. J. & Kim, H. S. A highly reliable copper nanowire/nanoparticle ink pattern with high conductivity on flexible substrate prepared via a flash light-sintering technique. *ACS Appl. Mater. Interfaces* **7**, 5674–5684 (2015).
31. Kanzaki, M., Kawaguchi, Y. & Kawasaki, H. Fabrication of conductive copper films on flexible polymer substrates by low-temperature sintering of composite Cu ink in air. *ACS Appl. Mater. Interfaces* **9**, 20852–20858 (2017).
32. Yim, M. J., Li, Y., Moon, K. S. & Wong, C. P. Oxidation prevention and electrical property enhancement of copper-filled isotropically conductive adhesives. *J. Electron. Mater.* **36**, 1341–1347 (2007).
33. Qi, S. et al. Copper conductive adhesives for printed circuit interconnects. In *IEEE 62nd electronic components and technology conference*. 1651–1655 (IEEE, 2012).
34. Kim, C. K., Lee, G. J., Lee, M. K. & Rhee, C. K. A novel method to prepare Cu@Ag core-shell nanoparticles for printed flexible electronics. *Powder Technol.* **263**, 1–6 (2014).
35. Lee, C., Kim, N. R., Koo, J., Lee, Y. J. & Lee, H. M. Cu-Ag core-shell nanoparticles with enhanced oxidation stability for printed electronics. *Nanotechnology* **26**, 455601 (2015).
36. Yu, J. H., Kang, K. T., Hwang, J. Y., Lee, S. H. & Kang, H. Rapid sintering of copper nano ink using a laser in air. *Int. J. Precis. Eng. Man.* **15**, 1051–1054 (2014).
37. Yu, M. H., Joo, S. J. & Kim, H. S. Multi-pulse flash light sintering of bimodal Cu nanoparticle-ink for highly conductive printed Cu electrodes. *Nanotechnology* **28**, 205205 (2017).
38. Liu, S., Tokura, R., Thanh Nguyen, M., Tsukamoto, H. & Yonezawa, T. Surfactant-stabilized copper paticles for low-temperature sintering: Paste preparation using a milling with small zirconia beads: Effect of pre-treatment with the disperse medium. *Adv. Powder Technol.* **31**, 4570–4575 (2020).
39. Peng, J. et al. Surface coordination layer passivates oxidation of copper. *Nature* **586**, 390–394 (2020).
40. Lin, J. Y., Neoh, K. G. & Teo, W. K. Thermogravimetry-FTIR study of the surface formate decomposition on Cu, CuCl, Cu_2O, and CuO-correlations between reaction selectivity and structural-properties. *J. Chem. Soc. Faraday T.* **90**, 355–362 (1994).
41. Dai, L. et al. Ultrastable atomic copper nanosheets for selective electrochemical reduction of carbon dioxide. *Sci. Adv.* **3**, e1701069 (2017).
42. Masashi, T. et al. Conductive copper paste, conductive copper paste cured film, and semiconductor device. *United State Pat. US10347388B2* (2018).
43. Takahashi, T. Resin composition, copper paste, and semiconductor device. *United State Pat. US10276277B2* (2018).
44. Lu, D. & Wong, C. P. Effects of shrinkage on conductivity of isotropic conductive adhesives. *Int. J. Adhes. Adhes.* **20**, 189–193 (2000).
45. Shahzad, F. et al. Electromagnetic interference shielding with 2D transition metal carbides (MXenes). *Science* **353**, 1137–1140 (2016).
46. Wang, Z. et al. Ultrahigh conductive copper/large flake size graphene heterostructure thin-film with remarkable electromagnetic interference shielding effectiveness. *Small* **14**, e1704332 (2018).
47. Koo, C. M., Sambyal, P., Iqbal, A., Shahzad, F. & Hong, J. *Two-Dimensional Materials for Electromagnetic Shielding* (John Wiley & Sons, 2021).
48. Kumar, P. et al. Large-area reduced graphene oxide thin film with excellent thermal conductivity and electromagnetic interference shielding effectiveness. *Carbon* **94**, 494–500 (2015).
49. Al-Ghamdi, A. A. & El-Tantawy, F. New electromagnetic wave shielding effectiveness at microwave frequency of polyvinyl chloride reinforced graphite/copper nanoparticles. *Compos. Part A* **41**, 1693–1701 (2010).
50. Al-Saleh, M. H., Gelves, G. A. & Sundararaj, U. Copper nanowire/polystyrene nanocomposites: Lower percolation threshold and higher EMI shielding. *Compos. Part A* **42**, 92–97 (2011).
51. Jiang, X. et al. Facile, green and affordable strategy for structuring natural graphite/polymer composite with efficient electromagnetic interference shielding. *RSC Adv.* **5**, 22587–22592 (2015).
52. Gargama, H., Thakur, A. K. & Chaturvedi, S. K. Polyvinylidene fluoride/nickel composite materials for charge storing, electromagnetic interference absorption, and shielding applications. *J. Appl. Phys.* **117**, 224903 (2015).
53. Li, L. & Chung, D. D. L. Electrical and mechanical-properties of electrically conductive polyethersulfone composites. *Composites* **25**, 215–224 (1994).
54. Kim, T. et al. Uniformly interconnected silver-nanowire networks for transparent film heaters. *Adv. Funct. Mater.* **23**, 1250–1255 (2013).
55. Huang, Q. et al. Highly flexible and transparent film heaters based on polyimide films embedded with silver nanowires. *RSC Adv.* **5**, 45836–45842 (2015).
56. Kellomaki, T., Virkki, J., Merilampi, S. & Ukkonen, L. Towards washable wearable antennas: A comparison of coating materials for screen-printed textile-based UHF RFID tags. *Int. J. Antenn. Propag.* **2012**, 476570 (2012).
57. Scarpello, M. L., Kazani, I., Hertleer, C., Rogier, H. & Vande Ginste, D. Stability and efficiency of screen-printed wearable and washable antennas. *IEEE Antenn. Wirel. Pr.* **11**, 838–841 (2012).

ACKNOWLEDGEMENTS

This work is dedicated to the 100th anniversary of Xiamen University. We acknowledge funding support from the National Natural Science Foundation of China (21805232, 22075238, 21890752, 21731005, 21721001, and 21905237), Science and Technology Projects of Innovation Laboratory for Sciences and Technologies of Energy Materials of Fujian Province (IKKEM) (1004-Y9122101), and the Tencent Foundation through the XPLORER PRIZE.

AUTHOR CONTRIBUTIONS

Each author's contribution to the paper is described as follows: B.W. conceived and supervised the research project. S.H., C.L., and S.H. synthesized and characterized the samples and investigated their anti-corrosion performance; these three authors were co-first authors and contributed equally to this work. S.H. conducted the calculations and simulations. W.F. and J.P. contributed to the sample preparations and characterizations. S.H. and C.L. wrote and revised the manuscript. B.W. and N.Z. contributed to project supervision and financial support.

COMPETING INTERESTS

Xiamen University has filed a patent (application No. CN202110840835.8) related to this work. All other authors declare no competing interests.

ADDITIONAL INFORMATION

Supplementary information The online version contains supplementary material available at https://doi.org/10.1038/s41528-022-00151-1.

Correspondence and requests for materials should be addressed to Binghui Wu.

Reprints and permission information is available at http://www.nature.com/reprints

Publisher's note Springer Nature remains neutral with regard to jurisdictional claims in published maps and institutional affiliations.

Open Access This article is licensed under a Creative Commons Attribution 4.0 International License, which permits use, sharing, adaptation, distribution and reproduction in any medium or format, as long as you give appropriate credit to the original author(s) and the source, provide a link to the Creative Commons license, and indicate if changes were made. The images or other third party material in this article are included in the article's Creative Commons license, unless indicated otherwise in a credit line to the material. If material is not included in the article's Creative Commons license and your intended use is not permitted by statutory regulation or exceeds the permitted use, you will need to obtain permission directly from the copyright holder. To view a copy of this license, visit http://creativecommons.org/licenses/by/4.0/.

© The Author(s) 2022